Results in Engineering 21 (2024) 101732

Contents lists available at ScienceDirect

Results in Engineering

journal homepage: www.sciencedirect.com/journal/results-in-engineering

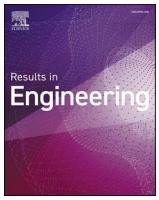

Case report

Experimental results for topologically optimised steel joints under tension

Tiago Ribeiro [a,*], Luís Bernardo [a], Miguel C.S. Nepomuceno [b], Natale Maugeri [c], Paolo Longo [c], Dario De Domenico [c]

[a] University of Beira Interior, Department of Civil Engineering and Architecture, 6201-001, Covilhã, Portugal
[b] University of Beira Interior, Department of Civil Engineering and Architecture, Centre of Materials and Building Technologies, 6201-001, Covilhã, Portugal
[c] Department of Engineering, University of Messina, 98166, Messina, Italy

ARTICLE INFO

Keywords:
Topology optimisation
Steel
Bolted connection
Tension
Ultimate capacity
Experimental validation

ABSTRACT

Developments on code-compliant Topology Optimisation methodologies for the steel construction industry have recently been proposed. Also, it has been found that topologically optimised steel bolted connection parts – which behave non-linearly to a very significant degree of damage – do not waive physically non-linear analyses to assess an ultimate capacity that can be lower than what is predicted by the optimisation procedure linear analyses. These two circumstances brought urgency to the experimental testing of such optimised parts. The herein depicted experimental programme assessed topologically optimised and previously numerically analysed bolted parts of a well-known steel connection. The results allowed redefining the material trilinear model to be used in further numerical analysis and, very significantly, validated the numerical simulations results as well as the application of Eurocode formulae for connections component resistance. The difference between the previous numerically predicted ultimate resistance and the experimentally defined did not exceed 2.6 %.

1. Introduction

Over the past thirty-five years, Topology Optimisation (TO) has benefited from the development of homogenisation methods [1–3] to enter an industry-prone modern age [4–7] which, ultimately, is paramount to foster the employment of sensible advances in the structural steel manufacturing processes optimisation [8–11]. Nevertheless, large-scale applications to the construction and civil engineering sectors are yet to be seen.

One of the main hindrances frequently pointed out for such an outcome is the lack of a code-compliant methodology that could merge the advanced calculations and cutting-edge software needed for TO with the very strict regulations that apply to construction [12]. Hence, recent research was promoted to address this issue, resulting in the development of a methodology [13–15].

Moreover, the same research also found that topologically optimised parts under an elastic domain tend to behave differently under the non-linear (post-elastic) regimen that shall be covered in the design and analysis of structural steel connections [14].

Under these circumstances, it became evident that the road towards practical applications of TO for the steel construction industry should include experimental testing, both static and dynamic, after the setting of a methodology and its validation with numerical analyses [16].

To meet such a stringent need regarding static experimental testing, an experimental programme was designed to physically test the prototypes designed with the recently proposed methodology based on current procedures for assessing the non-linear behaviour of steel parts [17]. The object of the optimisation procedure was the well-known Sheikh-Ibrahim's [18] connection, whose (non-optimised) behaviour has been thoroughly studied in the past.

Optimised tension cover-plates have consequently been produced through subtractive manufacturing and, along with material coupons to assess the prototypes' steel properties, tension tested. Endeavoured methodology can be briefly synthesised in a three-stage experimental protocol, with base material testing, sacrificial plates testing for layout assessment and, ultimately, prototypes testing.

The current document is, therefore, aimed at extensively depicting the experimental methods and their results, assessing the previous numerical findings [14], allowing correlations and conclusions to be accomplished, and enabling fellow researchers to use this work with full reproducibility.

The novelty brought by this document can be summarised in the

* Corresponding author.
E-mail addresses: tiago.pinto.ribeiro@ubi.pt (T. Ribeiro), lfb@ubi.pt (L. Bernardo), mcsn@ubi.pt (M.C.S. Nepomuceno), natale.maugeri@unime.it (N. Maugeri), paolo.longo@unime.it (P. Longo), dario.dedomenico@unime.it (D. De Domenico).

https://doi.org/10.1016/j.rineng.2023.101732
Received 12 September 2023; Received in revised form 17 December 2023; Accepted 29 December 2023
Available online 30 December 2023

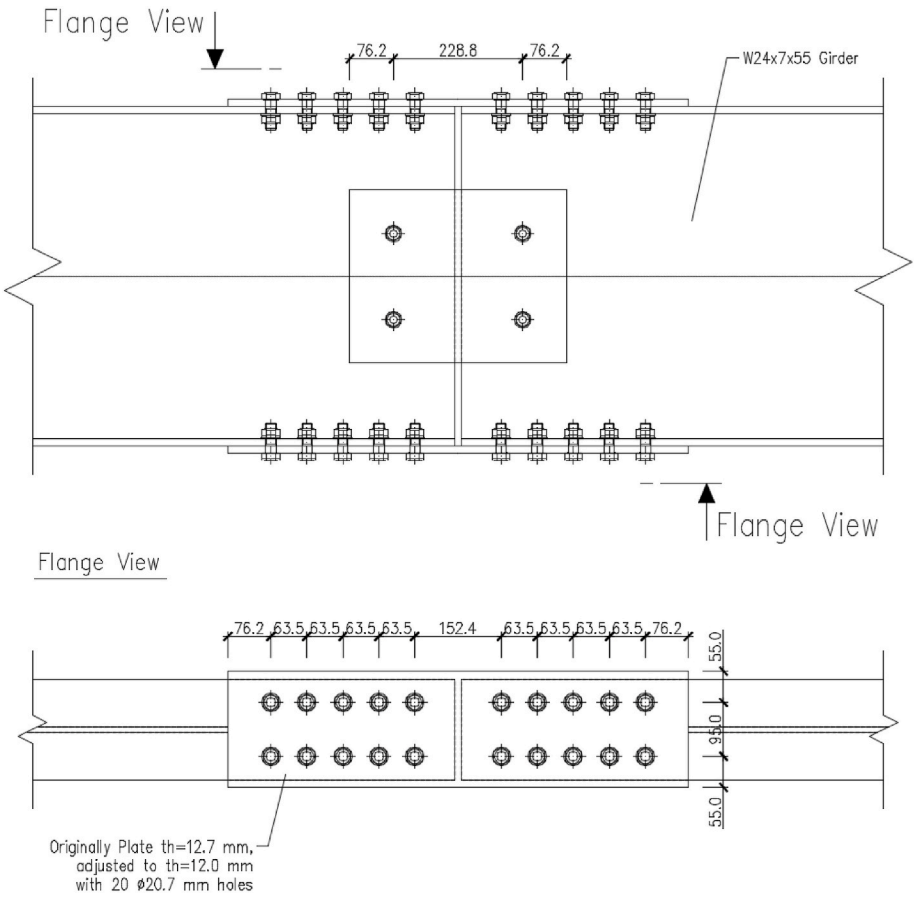

Fig. 1. Flange connection layout (dimensions in mm).

Table 1
Non-optimised plate failure modes and capacity parameters.

Component	Characteristic value	Design value	Notes
$F_{b,Rd}$	0.004620 f_u [kN] (with f_u in kPa)	0.003696 f_u [kN] (with f_u in kPa)	Flange cover-plate bearing resistance, according to Eurocode 3 [24] for Ultimate Limit States.
$F_{v,Rd}$	1176 kN	941 kN	Bolts shear resistance, according to Eurocode 3 [24] for Ultimate Limit States.
$N_{u,Rd}$	0.00176688 f_u [kN] (with f_u in kPa)	0.00141350 f_u [kN] (with f_u in kPa)	Plate's tensile resistance (net sectional area), according to Eurocode 3 [23,24] for Ultimate Limit States.

presentation of a rare topologically optimised connection plate testing to ultimate capacity, the validation of Eurocode design calculations with experimental values in optimised plates, extending the scope of application of such formulae and the proposition of a useful trilinear material model for non-linear analyses.

2. Materials

2.1. Sheikh-Ibrahim's splice connection

2.1.1. Geometry

The work of Sheikh-Ibrahim at the University of Texas at Austin, in 1995 [18], provided a comprehensive understanding of splice connections in steel girders and contributed to drafting design recommendations that became widely used by practitioners and researchers [19,20].

Therefore, the cases in this experimental programme were regarded as the ideal ground for employing a novel TO methodology. Sheikh-Ibrahim's Case 1 (out of 32) was considered and is illustrated in Fig. 1,

Table 2
Steel coupons and optimised prototypes parts list.

Part	Type	Manuf.	Steel Supply	f_y (ASTM A572-50)	f_u (ASTM A572-50)	f_y (Certif.)	f_u (Certif.)	Certif.
100 101 102 103 104 T1 T2 T3	Material Sample Optimised plate to 55 % vol. fract.	Valis	Çolakoglu lot 073335000 label 05685	345 MPa	450 MPa	439 MPa	563 MPa	99.TS.03.22. B1

Fig. 2. Steel coupons front and back. a) Part 100, b) Part 101, c) Part 102, d) Part 103 and e) Part 104.

Fig. 3. Optimised prototypes. a) Part T1, b) Part T2 and c) Part T3.

where two W24 × 7 × 55 segments in A36 steel [21] are joined with cover-plates (one in each flange and two in the web). As a result, A572 Grade 50 steel [22] flanges' cover-plates resist with simple shear. The flange cover-plates are 812.8 mm long, 205 mm wide and 12.7 mm thick. Since the manufacturing process was carried out in Europe, the plate thickness was adjusted to 12 mm.

The originally A325 steel twenty 19.1 mm diameter bolts were replaced with M20 (8.8) ones, complying with EN 14399 for the HR-tZn system. Bolt holes were adjusted to the European standards normal ones of 22 mm, and spaced of 63.5 mm in the longitudinal direction and 95 mm in the transversal one.

2.1.2. Original plate resistance

To set a baseline scenario for the non-optimised plate's expected failure modes, the European standards for steel construction were considered [23–25]. Component resistance, as per Eurocodes and proportionally to material strength, is enlisted in Table 1.

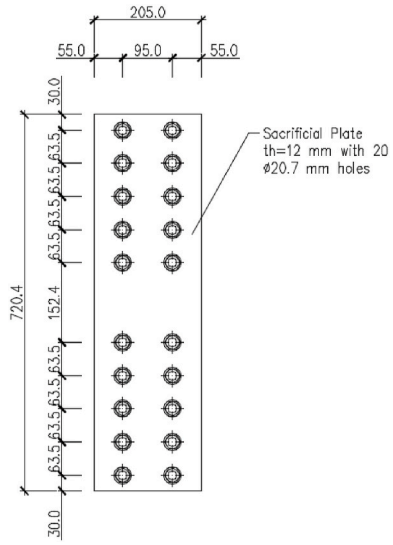

Fig. 4. Sacrificial test plate.

2.2. Topology Optimisation

The connections' tension plate was topologically optimised using a density-based approach, the Solid Isotropic Microstructure with Penalisation (SIMP) method [4] and a penalty factor of 3.

To such an end, a parametric study was pursued, with a proposed methodology described in Ref. [14], generating optimised topologies with volume fractions changing every 10 % from the original layout and, ultimately, every 5 % as solutions converged for optimality, to which physically non-linear analyses succeeded in finding each solution's exact ultimate capacity. Optimisation steps can also be found in Ref. [14].

The chosen topology has corresponded to the least volume fraction that has shown the ability to ensure the original connection's ultimate capacity.

2.3. Material model

The optimisation procedure was bound to consider the case study's flange plates material, which was, reportedly, Grade 50 steel according to the ASTM A572/A572 M standard [22]. This steel grade's mechanical properties are defined by a minimum yield strength of 345 MPa, a minimal ultimate strength of 450 MPa and a minimum elongation of 0.21 in a 50 mm gauge and 0.18 in a 200 mm gauge.

However, further parameters were needed to accomplish the non-linear analyses, such as information on the steel hardening phase and a realistic threshold for the ultimate elongation. Therefore, published literature was investigated, including Sheikh-Ibrahim's [18], Sheikh-Ibrahim and Frank's [19], Barbosa and Ruggieri's [26], Richter's [20] and Rex and Easterling's [27] publications, resulting in the ability to synthesise a realistic and code-supported trilinear model with hardening. Such a model is defined by an elastic stage with $E_0 = 199.9$ GPa, a plastic one with $E = E_0/339$ and a hardening one with $E = E_0/1000$ (as shown in Fig. 15).

Nevertheless, as the chosen topology reached the manufacturing stage, material models had to be adjusted to the real steel properties. The first insight was provided by the supplier material sheets. For the material batch of which the current plates were subtractively manufactured, Çolakoglu Metalurji ensured a yield strength of 439 MPa, an ultimate strength of 563 MPa and an elongation of 0.271 in a 200 mm gauge.

However, for a case-specific assessment, it has been considered that

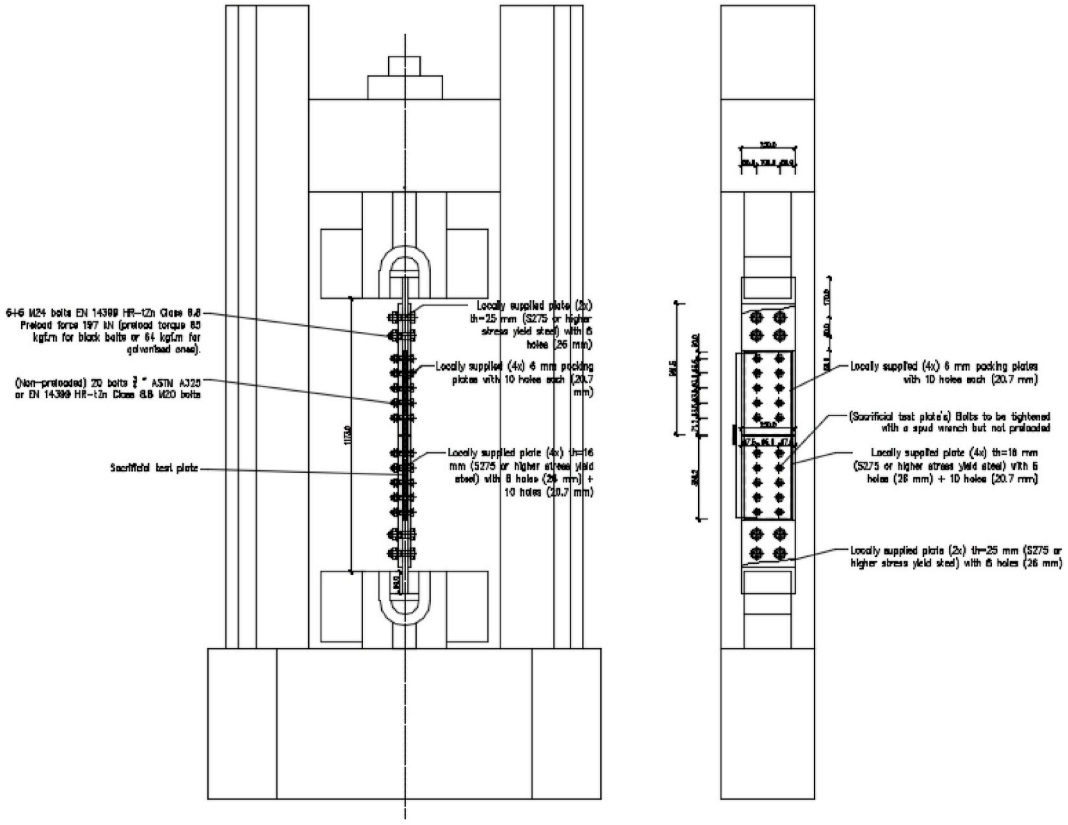

Fig. 5. Testing layout for the sacrificial test plate.

steel coupons gathered from the steel plate should be analysed. Those results are presented in a following section and used to attain the adjusted trilinear model with hardening, as depicted in Fig. 15.

2.4. Manufactured parts

2.4.1. Steel coupons

Five material samples were taken from the steel plate used to materialise the optimised prototypes. These coupons, listed in Table 2 and shown in Fig. 2, were retrieved in a prismatic shape and subsequently prepared to match the gauges defined for material testing.

2.4.2. Optimised prototypes

In order to ensure statistical value to the conclusions that can be drawn from the testing of the optimised solutions, three identical prototypes have been manufactured. The prototype list and photographic report are depicted in Table 2 and Fig. 3, respectively.

3. Experimental methods

3.1. Experimental protocol

The experimental protocol can be defined as a three-staged one, including the prototypes material testing through steel coupons, the layout testing with sacrificial plates and, finally, the prototypes testing.

Concerning the first stage, to ensure that the test results are admissible both under European (EN 10025-2) and American (ASTM A572) materials standards, the test section is defined as 12 mm × 6 mm, and the test length is 50 mm. A "*gauge*" is necessary to limit the yielding section. The minimal number of results to provide characteristic values for the steel properties assessment has been valued in three. However, five specimens were manufactured to ensure the test robustness and tolerance to unforeseeable events, of which four coupons were prepared and tested.

A test with a "*sacrificial test plate*" will follow to assess the testing layout, measurement display and testing conditions, to ensure the personnel training in the assembly sequence and testing recording, to investigate possible errors in the setup and to ascertain the general conditions for the subsequent prototypes testing. The "*sacrificial test plate*" is depicted in Fig. 4, and the testing layout is shown in Fig. 5.

After implementing any adjustment regarded as necessary after analysing the sacrificial plate testing data, the layout for the prototypes is assembled, as illustrated in Fig. 6, and the tests were carried out.

3.2. Testing of steel coupons

Four "gauge" testing specimens were manufactured from the prismatic coupons. The procedure endeavoured to attain these specimens is described in Fig. 7, and its goal was ensuring 50 mm long testing gauges with a 12 mm × 6 mm section.

These specimens were tested until failure to determine the yielding stress, the ultimate stress, and the ultimate strain of the material. All the tests were performed in displacement-control mode using a monotonic ramp with a displacement rate equal to 0.05 mm/min, per the literature on steel bolted connections [28,29].

The testing equipment used for the tests was a universal testing machine, "*MTS 810 Material Test System, model 318.25*", having a load capacity of 250 kN and clamping maximal pressure of 69 MPa. The strain of the "gauge" specimens was measured not only through the crosshead motion, assuming a uniform deformation along the 50 mm length of the reduced section ("*crosshead def*"), but also through an integrated extensometer MTS 634.12F-24, S/N 10183942E with gauge length equal to 25 mm ("*extensometer def*"). A schematic picture of the testing machine is illustrated in Fig. 8.

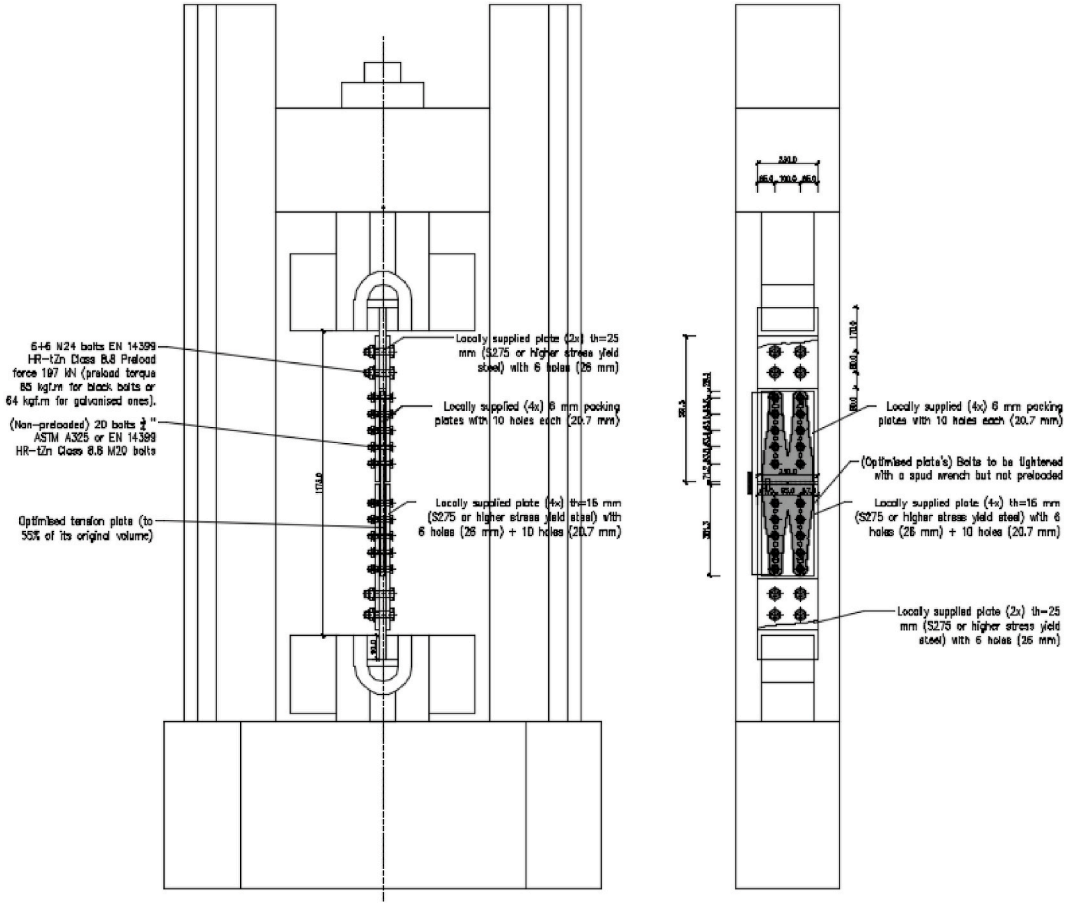

Fig. 6. Testing layout for the prototypes.

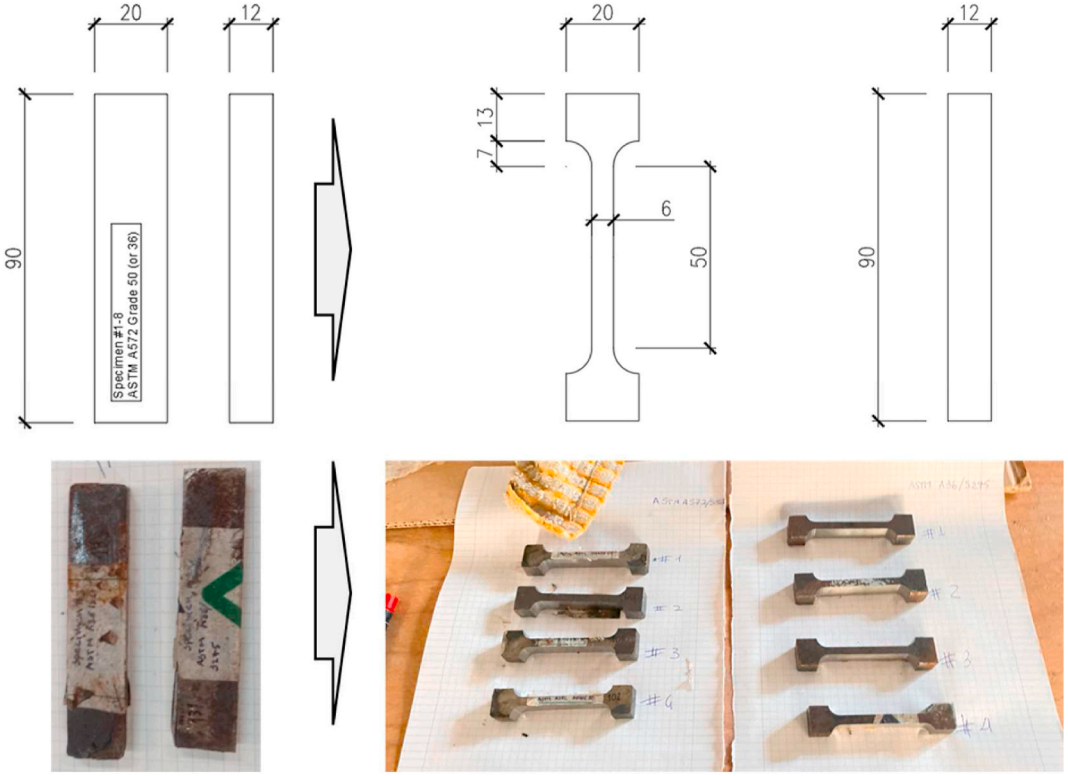

Fig. 7. Drawings and photographs of steel coupons tested for material characterisation (units in [mm]).

Fig. 8. Testing equipment used for the tensile tests on steel coupons for material characterisation.

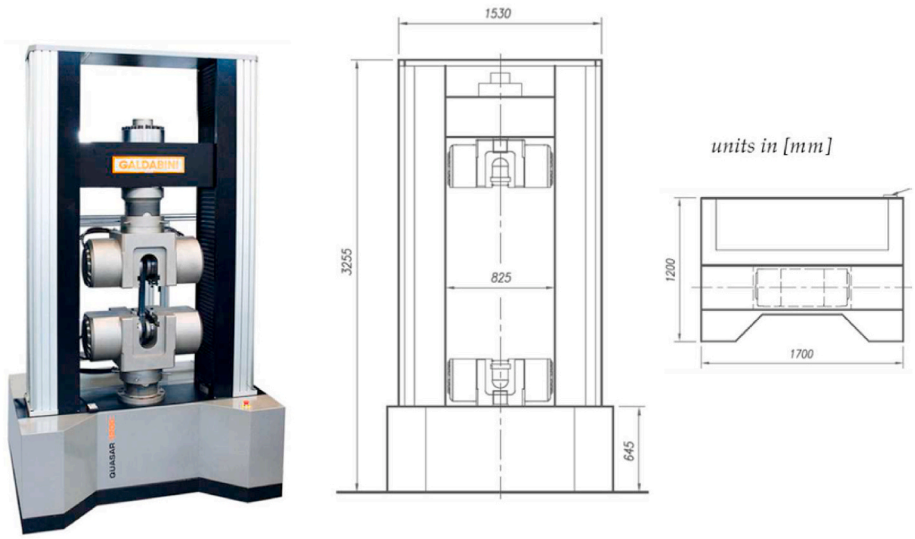

Fig. 9. Testing equipment used for the tests on the steel connection prototypes.

3.3. Testing of steel prototypes and sacrificial plates

The tests on the optimised tension plate prototypes were performed in displacement control mode using a monotonic ramp with a displacement rate equal to 1 mm/min, per the literature on steel bolted connections [28,29].

The testing equipment used for the tests is a universal testing machine model "*Galdabini Quasar 1200 S/N VB47*", having a nominal load capacity of 1200 kN, total stroke of 1300 mm, and clamping maximum force of 1800 kN. A schematic picture of the testing machine is illustrated in Fig. 9, and the assembly process is illustrated in Fig. 10.

In addition to the integrated measurement of the machine frame vertical motion ("*crosshead*"), the local deformation of the tested specimens was computed with the aid of two linear variable displacement transducers (LVDTs), model "*Monitran MTN/IEUSAL050-10*", having stroke ± 50 mm, placed according to a suitable configuration as shown in Fig. 11 for the tensile tests. The latter displacement measurement is labelled as "*LVDT*" and is the difference between the displacement measured by LVDT1 and that measured by LVDT2. It is expected that the displacement measurement obtained through the two LVDTs represents the net displacement of the specimen, while that obtained via the crosshead motion represents the gross displacement of the overall test setup, which might be affected by minor slip phenomena at the wedges and other slips caused by bolt-hole clearance.

The two LVDTs were placed on the two sides of the tested specimen so that their spring-terminals point towards a cubic magnet fixed on the auxiliary plates just beyond the prototype's length. In this way, the actual elongation of the prototype was measured as the difference between the two absolute values recorded by the two LVDTs, thus eliminating in the measurement any slips occurring in the gripping area at the

Fig. 10. Assembly process.

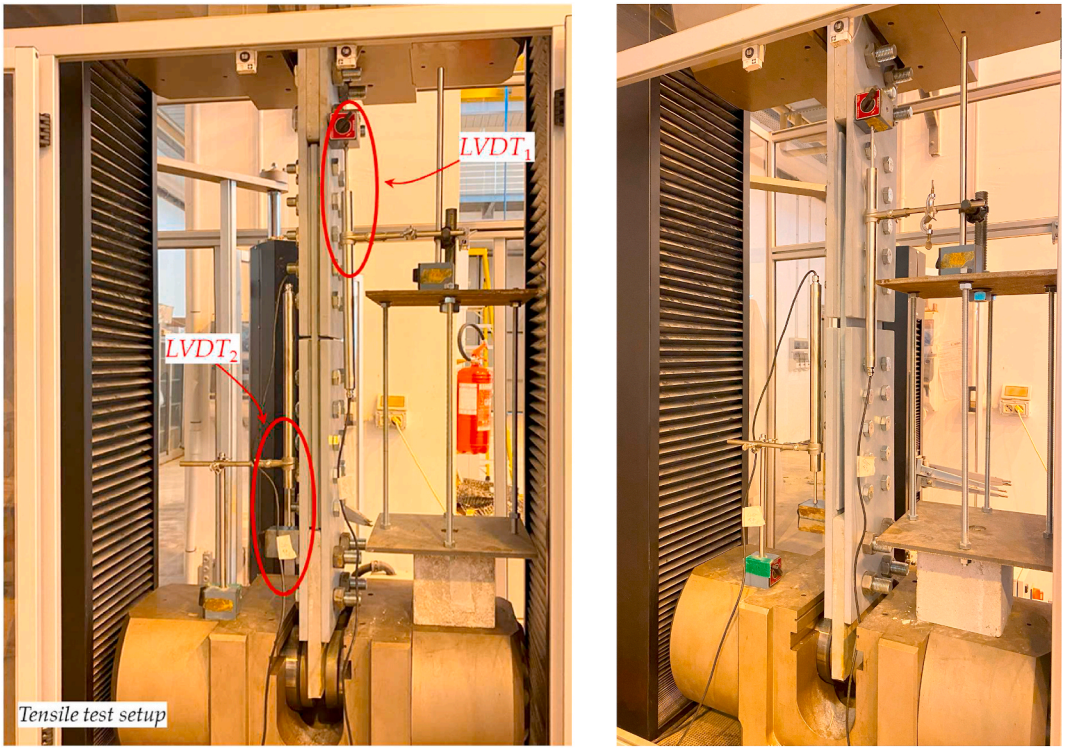

Fig. 11. Configuration of LVDTs used for the tensile tests.

wedges or any bolt-holt clearance occurring in the fixing M27 bolts.

The two LVDT measurements are obtained through an acquisition unit model "*NI cDAQ 9189*", equipped with an appropriate connector type "NI-9209" for measuring input voltage signals. A customised "*project*" has been realised in the LabView programming environment to convert, in real-time, the voltage signal into a displacement signal (through a calibration constant provided by the LVDT manufacturer) and to save all the recorded signal in a. txt file for postprocessing purposes. All the measurements (those related to the crosshead motion as well as those obtained through the LVDTs) are obtained at a sampling frequency equal to 10 Hz.

4. Results and discussion

4.1. Tensile tests on steel coupons for material characterisation

The tensile test results on the steel coupons, in terms of stress-strain curves for crosshead deformation and extensometer deformation, are depicted in Fig. 12 for the material ASTM A572-50. It shall be noted that, for coupon 2, the extensometer detached abruptly at failure, leading to the abnormal phenomenon reported in Fig. 12. A comparison between the four stress-strain curves obtained for the four specimens (crosshead deformation) is illustrated in Fig. 13. The yielding and ultimate stress obtained for the four specimens, the mean value, and the coefficient of variation (CoV) are listed in Table 3.

Hence, the yield stress, which ASTM A572-50 inferiorly bounds in 345 MPa, has been described as 439 MPa in the material certificate and experimentally defined as 364.9 MPa (CoV 0.9 %). Moreover, the ultimate stress, inferiorly bounded by ASTM A572-50 in 450 MPa, has been described as 563 MPa in the material certificate and experimentally defined as 508.5 MPa (CoV 1.9 %).

With regard to the failure mode, the collapse of the steel coupons occurred in the central part of the "gauge" specimen, preceded by an evident steel necking phenomenon, as observed in the photographs reported in Fig. 14.

Considering the experimental results, the material stress-strain diagram was adjusted employing numerical methods [30–32]. Yield and ultimate stress were defined to the observed values, E_0 was kept at 199.9

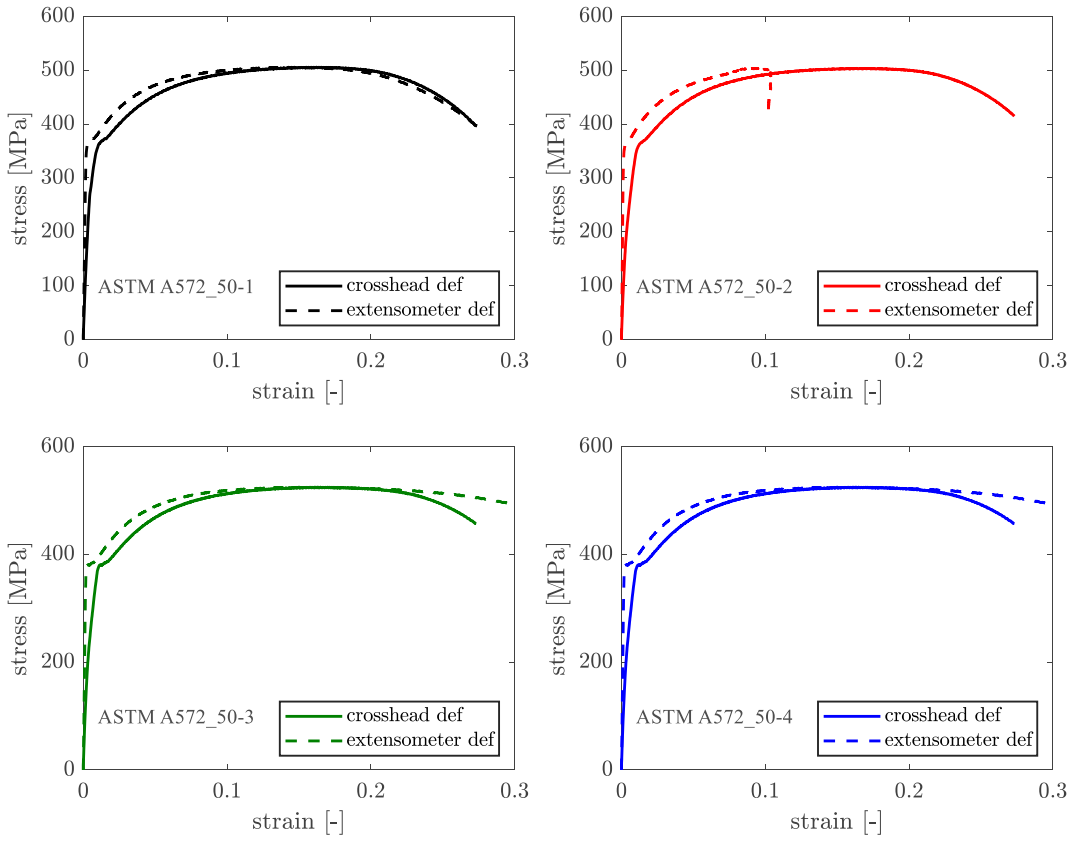

Fig. 12. Stress-strain curves of four ASTM A572-50 steel coupons.

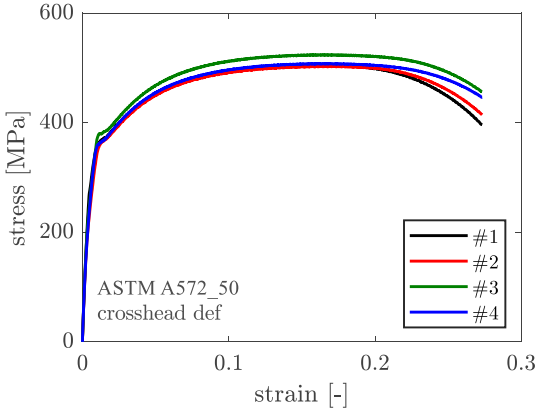

Fig. 13. Comparison of the four stress-strain curves of ASTM A572-50.

Table 3
Yielding and ultimate stress as well as ultimate strain, determined by tensile tests on steel coupons.

Coupon	ASTM A572-50			
	f_y [MPa]	f_u [MPa]	$\varepsilon_{u,ext}$ [−]	$\varepsilon_{u,crosshead}$ [−]
100	363.8	503.8	0.147	0.162
101	369.7	501.2	0.091	0.163
102	363.8	522.4	0.163	0.171
103	362.4	506.4	0.157	0.171
mean	**364.9**	**508.5**	**0.139**	**0.170**
CoV (%)	0.88	1.87	23.62	2.97

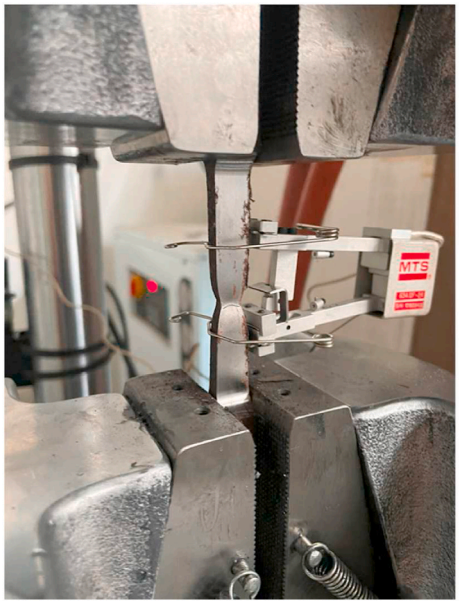

Fig. 14. Representative failure of steel coupons made of ASTM A572-50.

GPa, and, for the hardening stage, E was limited to $E_0/10000$ to avoid the non-negligible excess of the experimentally determined ultimate stress. The plastic stage's Young modulus was adjusted to $E = E_0/192$. Fig. 15 shows both the original stress-strain diagram used in numerical analyses [13,14], and the one adjusted after the experimental findings.

Fig. 15. Steel stress-strain diagrams.

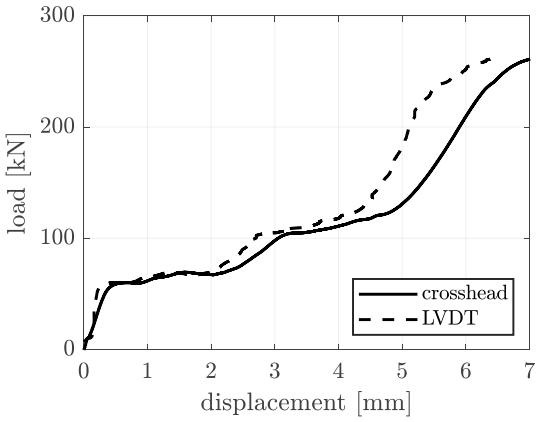

Fig. 16. Load-displacement graph of the sacrificial test plate under tension.

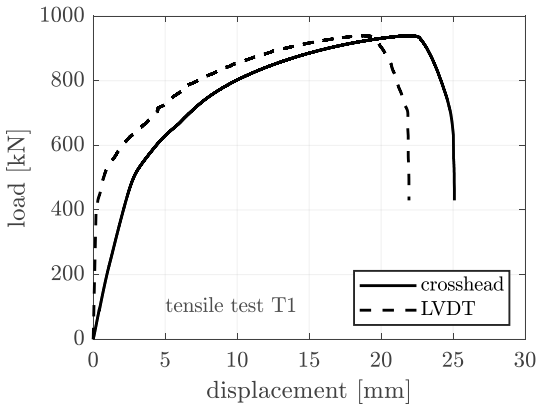

Fig. 18. Load-displacement graph of the tensile plate T1.

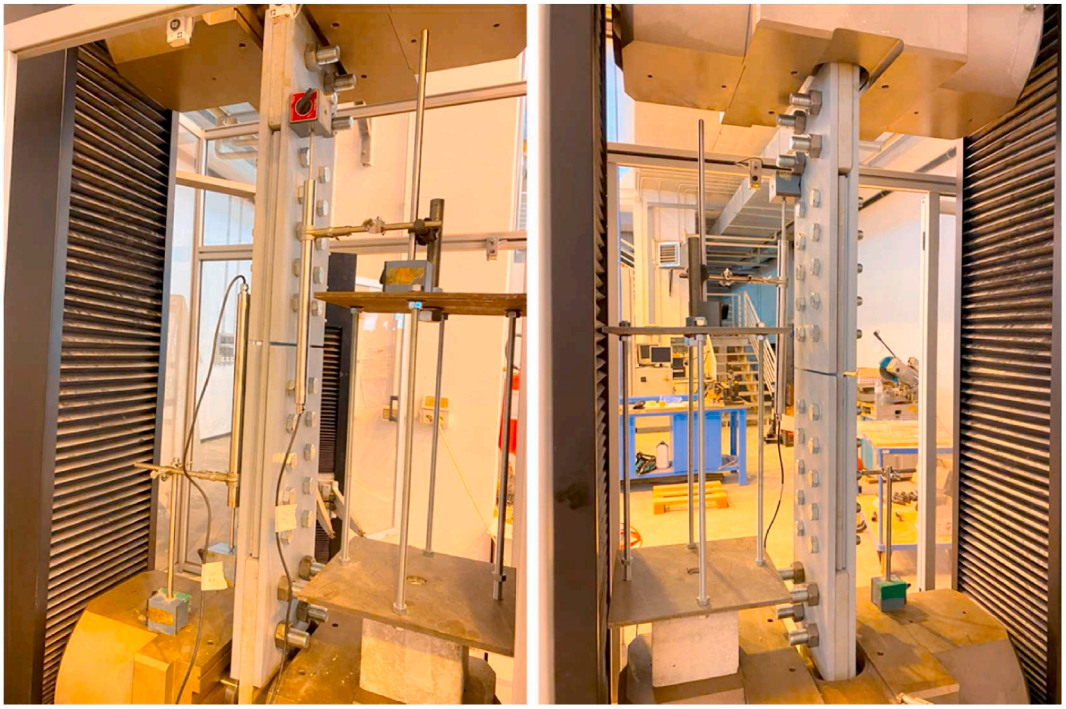

Fig. 17. Sacrificial plate during the tests.

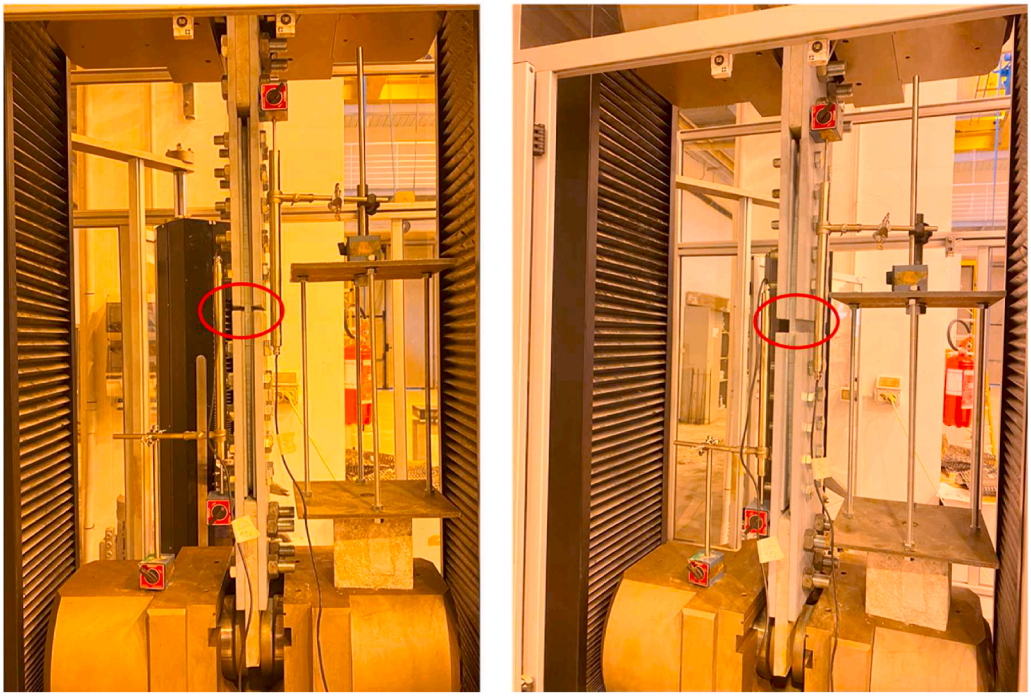

a) b)

Fig. 19. Tensile test on specimen T1. a) Specimen at the beginning of the test, b) Specimen under increasing deformation.

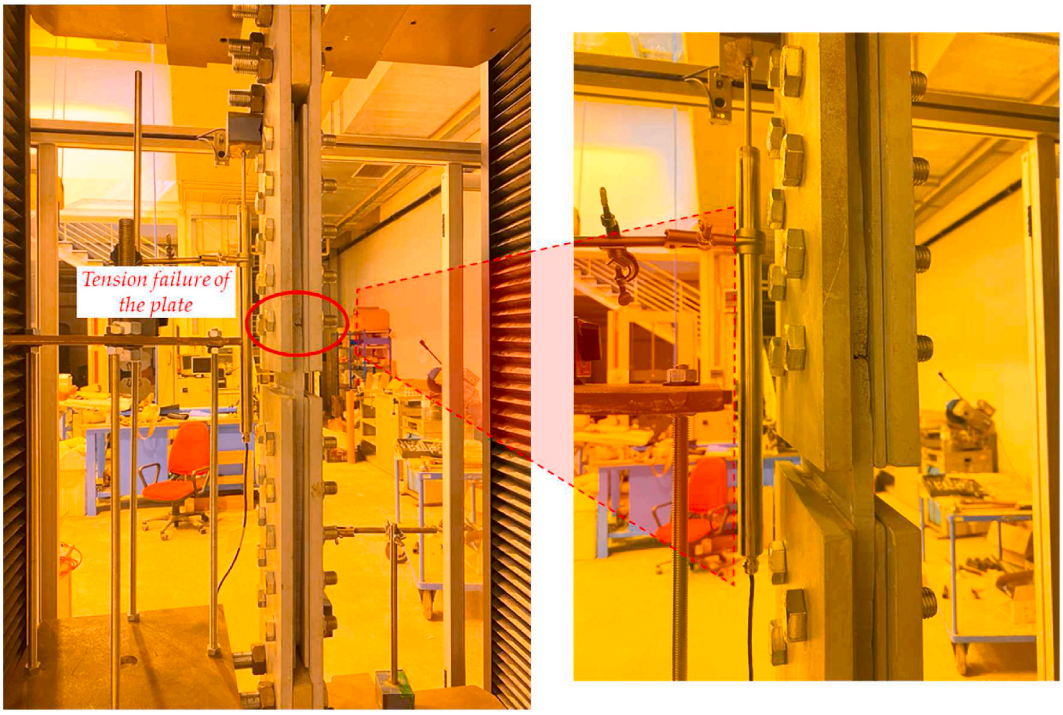

Fig. 20. Failure of prototype T1 while being in the testing machine.

4.2. Tensile tests on sacrificial test plates for calibration of tension laboratory setup

The purpose of this test is to assess if there is anything wrong with the layout, geometry and other assumptions that may lead to unintended behaviour; the base scenario for a non-optimised plate and its failure mode characterisation; the measurement display (LVDT) behaviour, installation, quantity and sufficiency; and the personnel training for performing the following tests and recording.

The tests were performed by tightening the 4 + 4 M27 bolts (at the terminal fixed plates) by applying the required preload torque of 64 kgf. m (627.6 Nm) and by manually tightening with a spud wrench the 10 + 10 M20 bolts (of the sacrificial test plate) without any applied preload.

The test was not meant to cause any damage to the sacrificial test

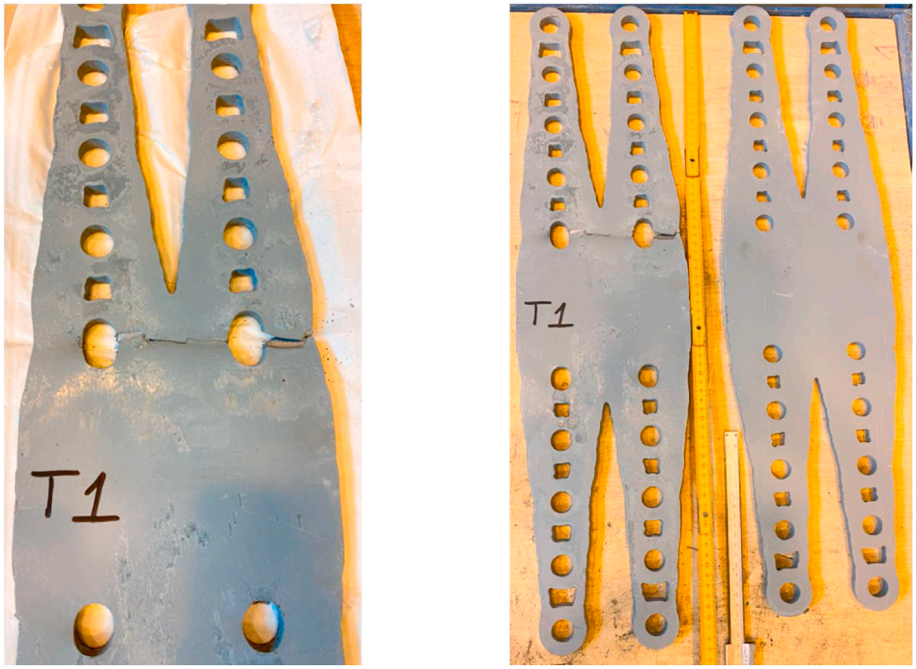

Fig. 21. Failure of prototype T1 extracted from the testing machine.

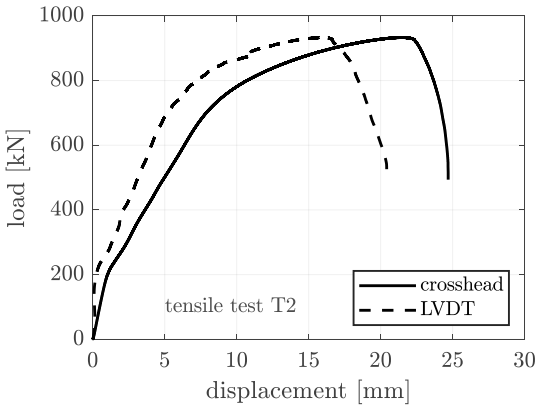

Fig. 22. Load-displacement graph of the prototype T2.

plate (as the same plate shall be re-used in future test setups). Based on the expected ultimate load of the optimised plate, the test was stopped at a load approximately equal to 250 kN, deemed sufficient for checking the correct configuration for the testing setup and acquisition system.

The load-displacement graph of the sacrificial test plate under tension is reported in Fig. 16.

The crosshead motion (whose measure is integrated into the machine setup) and the external LVDT measurements (obtained through the external acquisition unit "*NI cDAQ 9189*") are relatively consistent. When the sacrificial plate is pulled, the connection slips and the bolts shank contacts with the holes' borders. This behaviour is observed in the load-displacement graph that exhibits some plateau branches in terms of crosshead motion and LVDT measurements. This behaviour can be prevented by pulling the specimen before the test until a slight load increase (50–100 kN) is observed and then releasing the specimen until the force measured by the load cell returns to zero. Some photographs of the sacrificial plates during the tests are shown in Fig. 17.

4.3. Tensile tests on the optimised bolted connections' prototypes

Three tensile tests were performed on three identical specimens. The 10 + 10 M20 bolts were tightened to reduce the bolt-hole clearance at the beginning of the tests. Moreover, a preliminary pulling (while keeping the specimen in the elastic stage) was applied until the load was equal to 100 kN to ensure all the bolts' shank contacts with the holes' borders at the beginning of the test.

The results of the first prototype (T1) in terms of load-displacement curves are reported in Fig. 18. The specimen failed at a load equal to 939.3 kN, corresponding to a displacement of 21.97 mm (measured through the crosshead motion) and 18.83 mm (measured through the LVDTs).

Some photographs of the tensile test on specimen T1 are reported in Fig. 19, while the failure of the specimen is illustrated in Figs. 20 and 21. In particular, the deformations are concentrated along the holes' borders (which tend to elongate along the loading direction) and are more pronounced in the pairs of holes closer to the centre of the specimen, which has the largest (stiffest) section. Plate material becomes upset and piles up around the hole in the area of plate-bolt contact. The rupture section intersects the holes' row in the upper part of the specimen and reaches the specimen edge only on one side (Fig. 21).

The results of the second prototype (T2) in terms of load-displacement curves are reported in Fig. 22. The prototype failed at a load equal to 933.1 kN, corresponding to a displacement equal to 21.52 mm (measured through the crosshead motion) and 15.91 mm (measured through the LVDTs).

Some photographs of the tensile test on prototype T2 are reported in Fig. 23, while the failure of the prototype is illustrated in Figs. 24 and 25. In particular, the deformations are concentrated along the holes' borders (which tend to elongate along the loading direction) and are more pronounced in the pairs of holes closer to the centre of the prototype, which has the largest (stiffest) section. The rupture section intersects the holes' row in the lower part of the prototype and reaches the prototype edge on both sides (Fig. 25), which is different from what was observed in prototype T1. Unlike the prototype T1, the failure affects the entire cross-section of the plate.

The results of the third specimen (T3) in terms of load-displacement curves are reported in Fig. 26. The specimen failed at a load equal to 848.8 kN, corresponding to a displacement of 19.34 mm (measured through the crosshead motion) and 15.74 mm (measured through the LVDTs).

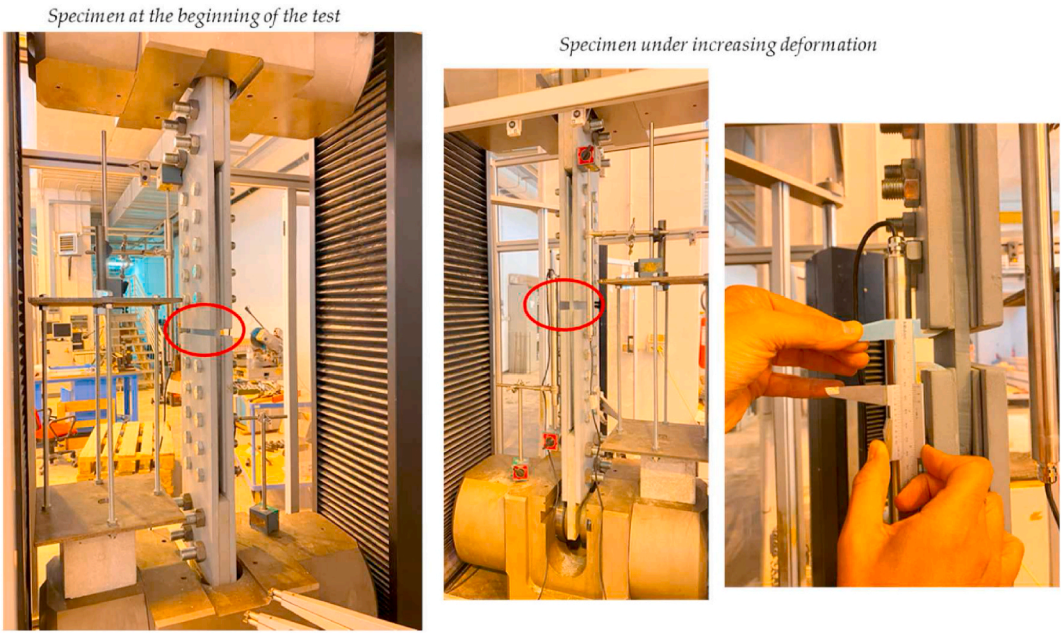

Fig. 23. Tensile test on specimen T2.

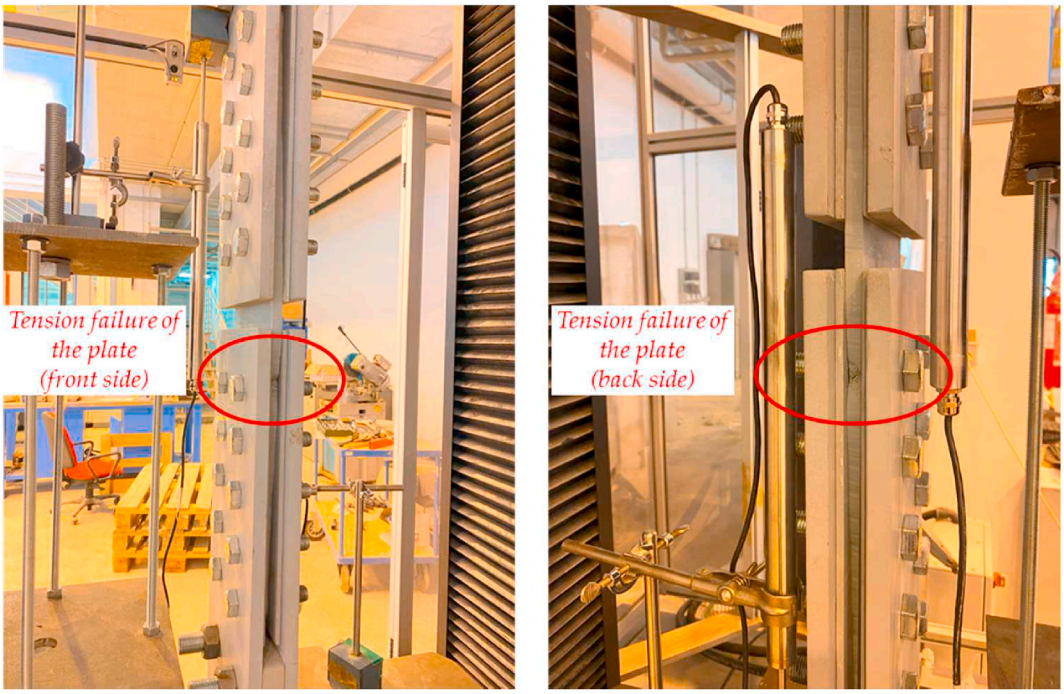

Fig. 24. Failure of specimen T2 while being in the testing machine.

Some photographs of the tensile test on specimen T3 are reported in Fig. 27, while the failure of the specimen is illustrated in Figs. 28 and 29. In particular, the deformations are concentrated along the holes' borders (which tend to elongate along the loading direction) and are more pronounced in the pairs of holes closer to the centre of the specimen, which has the largest (stiffest) section. The rupture section intersects the holes' row in the upper part of the specimen and reaches the specimen edge only on one side (Fig. 29), similar to what was observed in specimen T1. As for the specimen T1, the rupture partially affects the cross-section of the plate.

A summary of the test results on the three tested prototypes, T1, T2 and T3, is listed in Table 4 and in Fig. 30, in which a good repeatability of the test results among the three prototypes is observed (small dispersion, especially in terms of maximum load).

Experimental results characterised the prototypes' ultimate capacity as 907.1 kN (CoV 5.6 %). These values compare with the adjusted ultimate capacity of the optimised plate. Hence, once the plate resistance is adjusted to consider the thickness of 12.0 mm instead of 12.7 mm and to the yield and ultimate stresses of 365 and 509 rather than the code-based values of 345 and 450 MPa, respectively, the prototypes became expected to reach a global ultimate characteristic resistance of 898 kN considering the Eurocode-defined collapse mechanisms and 884 kN considering the numerical analyses [14]. Hence, experimental results match the Eurocode formulae computations for characteristic values,

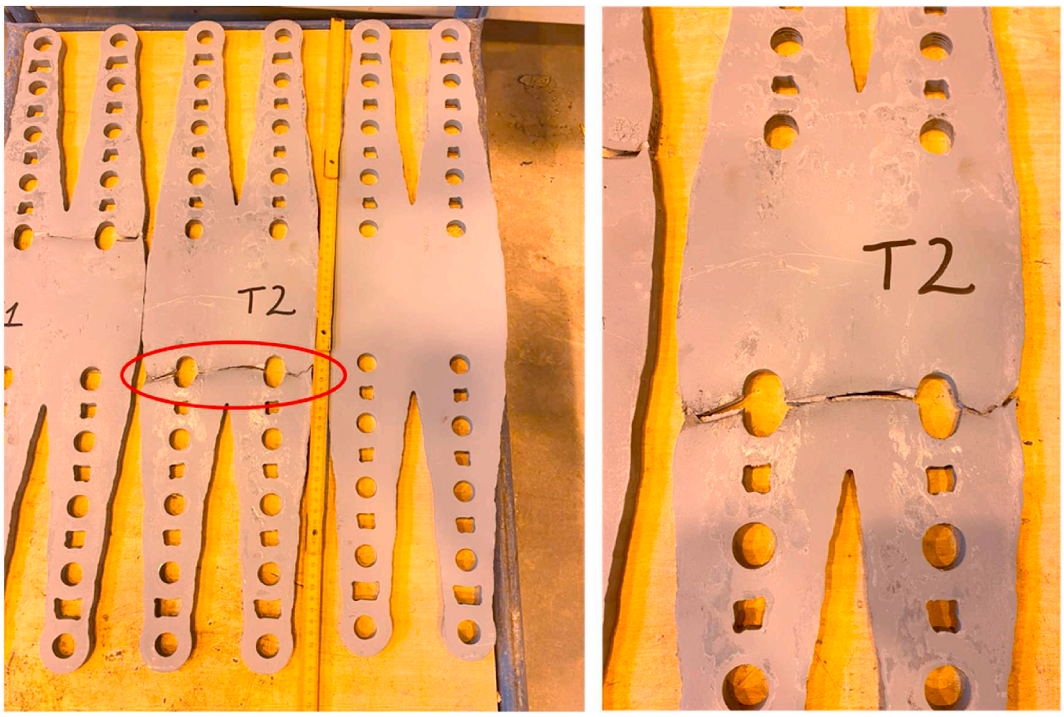

Fig. 25. Failure of specimen T2 extracted from the testing machine.

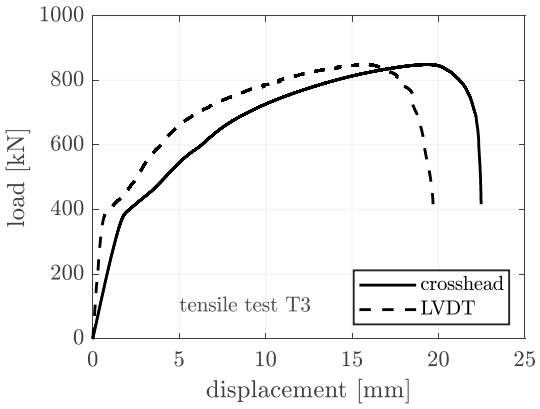

Fig. 26. Load-displacement graph of the tensile plate T3.

after the aforementioned properties adjustment, suggesting that the Eurocode safety margins will be valid also for the current topologically optimised parts.

5. Conclusions

An experimental programme assessed the behaviour of topologically optimised steel connection plates and provided helpful information on the validity of previous numerical physically non-linear analyses performed on those elements.

Tension tests were performed on steel coupons extracted from the base material with which the optimised prototypes were manufactured. The resulting experimental data allowed the synthesis of a new trilinear material model, which can be of significant worth for future numerical analyses in the optimised parts.

The experimentally determined ultimate capacity of the prototypes remarkably resembled the predicted values. Not only did the experimental ultimate capacity slightly exceed the numerical simulations results and the standard-defined characteristic values, which are regarded as crucial for attesting the TO procedure as safe-sided for engineering design, but it surpassed those values by 2.6 % and 1.0 %, respectively, validating the numerical results.

The fact that Eurocode formulae for computing the plate characteristic ultimate resistance does not deviate from the experimental results by more than 1.0 % is a critical conclusion since it supports the use of Eurocode for topologically optimised solutions, provided that the methodology proposed in Ref. [14] is followed and, thus, extending the Eurocode scope of application.

Future developments of the current study include revising numerical analyses considering the proposed steel trilinear model and the plate's adjusted thickness. Yet, releasing a detailed results article at this stage allows the community to replicate or proceed with autonomous research, making good use of a technically challenging and expensive testing programme.

Funding

Centre of Materials and Building Technologies (C-MADE) is thanked for funding the manufacture of the first batch of optimised plates, covering the costs of local supplies, and funding technical assistance to laboratory activities. C-MADE expenses are supported with Portuguese national funds by FCT - Foundation for Science and Technology, I.P., within the project C-MADE- UIDB/04082/2020.

CRediT authorship contribution statement

Tiago Ribeiro: Conceptualization, Formal analysis, Funding acquisition, Investigation, Methodology, Resources, Validation, Visualization, Writing - original draft, Writing - review & editing. **Luís Bernardo:** Funding acquisition, Resources, Supervision. **Miguel C.S. Nepomuceno:** Funding acquisition, Resources, Supervision. **Natale Maugeri:** Data curation, Investigation, Resources. **Paolo Longo:** Data curation, Investigation, Resources. **Dario De Domenico:** Data curation, Investigation, Resources, Supervision.

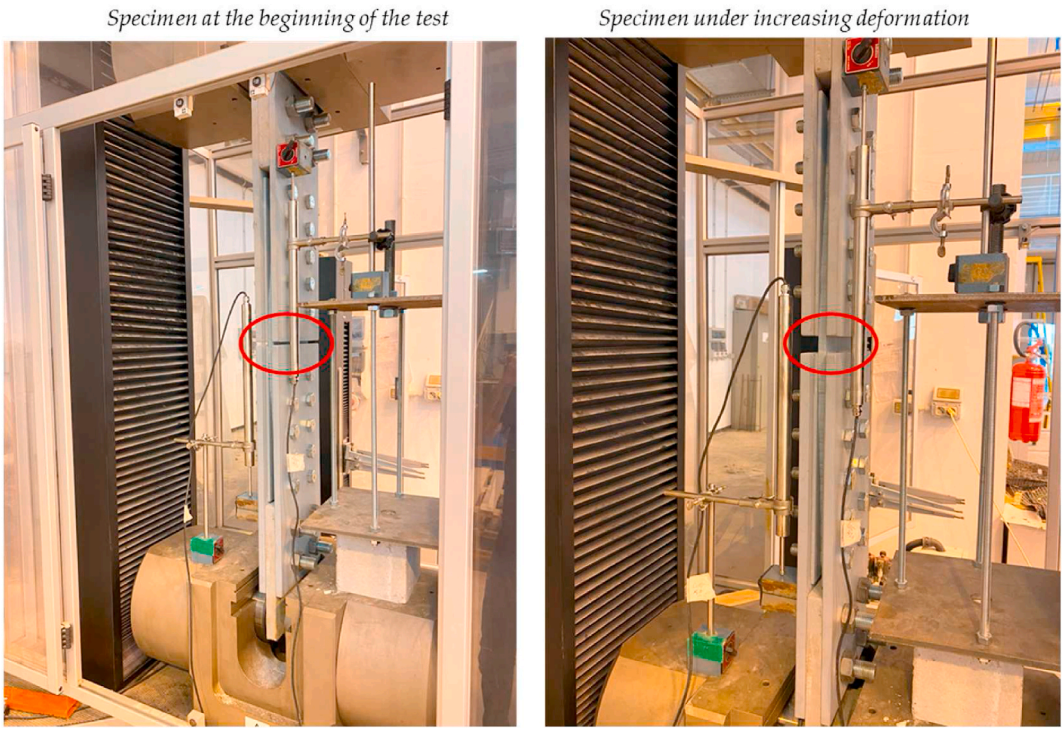

Fig. 27. Tensile test on specimen T3.

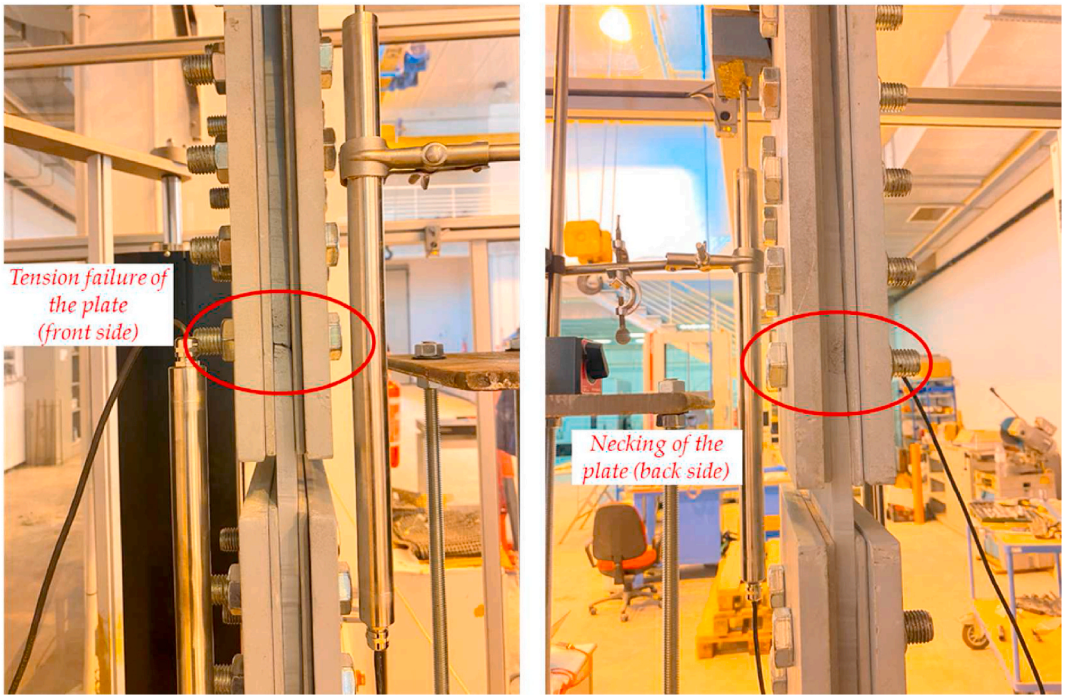

Fig. 28. Failure of specimen T3 (tensile plate) while being in the testing machine.

Declaration of competing interest

- All authors have participated in (a) conception and design, or analysis and interpretation of the data; (b) drafting the article or revising it critically for important intellectual content; and (c) approval of the final version.
- This manuscript has not been submitted to, nor is under review at, another journal or other publishing venue.
- The authors have no affiliation with any organization with a direct or indirect financial interest in the subject matter discussed in the manuscript

Data availability

Data is fully depicted in the article

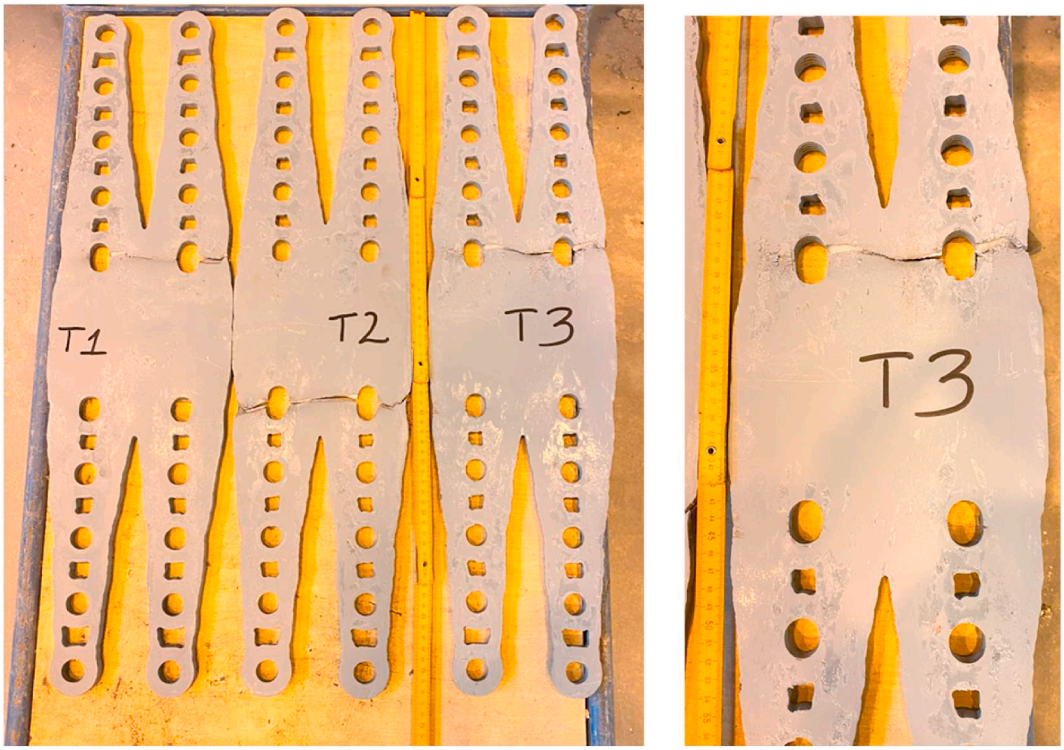

Fig. 29. Failure of specimen T3 (tensile plate) extracted from the testing machine.

Table 4
Peak load and displacement for the three prototypes.

Prototype	Peak load [kN]	Displacement at peak load [mm]	
		crosshead	LVDT
T1	939.3	21.97	18.83
T2	933.1	21.52	15.91
T3	848.8	19.34	15.74
Mean	**907.1**	**20.94**	**16.83**
CoV (%)	5.57	6.72	10.32

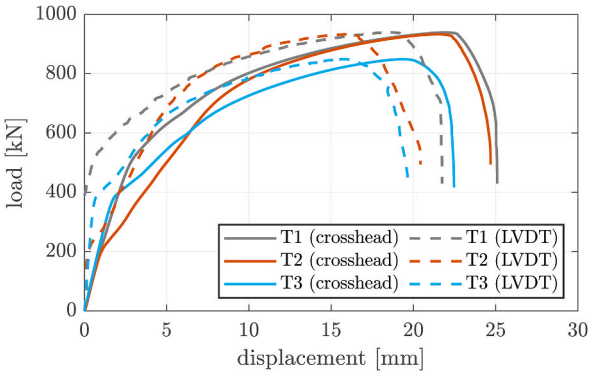

Fig. 30. Comparative plot for the three prototypes.

Acknowledgements

VALIS Engineering and HERMAF – Construções Metalomecânicas, Máquinas e Ferramentas, Lda. are thanked for supporting the manufacture of two additional batches of testing plates. Professors Chiara Borsellino, Giuseppe Ricciardi, and Ms. Federica Favaloro are thanked for their help with the laboratory activities within the University of Messina.

References

[1] M.P. Bendsøe, N. Kikuchi, Generating optimal topologies in structural design using a homogenisation method, Comput. Methods Appl. Mech. Eng. 71 (1988) 197–224.
[2] M.P. Bendsøe, Optimal shape design as a material distribution problem, Struct. Optim. 1 (1989) 193–202, https://doi.org/10.1007/BF01650949.
[3] K. Suzuki, N. Kikuchi, Shape and topology optimisation by a homogenisation method, Am. Soc. Mech. Eng. Appl. Mech. Div. AMD. 115 (1990) 15–30.
[4] T. Ribeiro, L. Bernardo, J. Andrade, Topology optimisation in structural steel design for additive manufacturing, Appl. Sci. (2021), https://doi.org/10.3390/app11052112.
[5] M.P. Bendsøe, O. Sigmund, Topology Optimization - Theory, Methods, and Applications, Springer, 2012, https://doi.org/10.1007/978-3-7091-1309-7_3.
[6] R.T. Haftka, Z. Gurdal, Elements of Structural Optimization, Kluwer Academic Publishers, 2002.
[7] G.I.N. Rozvany, T. Lewiński, Topology Optimization in Structural and Continuum Mechanics, 2014.
[8] M.A. Obeidi, Metal additive manufacturing by laser-powder bed fusion:Guidelines for process optimisation, Results Eng 15 (2022), 100473, https://doi.org/10.1016/j.rineng.2022.100473.
[9] A.M. Adem, H.E. Azmeraw, The manufacturing practices and parameters optimisation on abrasive jet machining for surface preparation of mild steels, Results Eng (2022), https://doi.org/10.1016/j.rineng.2022.100457.
[10] O.S. Ogbonna, S.A. Akinlabi, N. Madushele, O.S. Fatoba, E.T. Akinlabi, Grey-based taguchi method for multi-weld quality optimisation of gas metal arc dissimilar joining of mild steel and 316 stainless steel, Results Eng (2023), https://doi.org/10.1016/j.rineng.2023.100963.
[11] A.J. Santhosh, A.D. Tura, I.T. Jiregna, W.F. Gemechu, N. Ashok, M. Ponnusamy, Optimization of CNC turning parameters using face centred CCD approach in RSM and ANN-genetic algorithm for AISI 4340 alloy steel, Results Eng (2021), https://doi.org/10.1016/j.rineng.2021.100251.
[12] T. Ribeiro, L. Bernardo, R. Carrazedo, D. De Domenico, Seismic design of bolted connections in steel structures — a critical assessment of practice and research, Buildings (2022).
[13] T. Ribeiro, L. Bernardo, R. Carrazedo, D. De Domenico, Eurocode-compliant topology optimisation and analysis of a steel cover-plate in a splice moment connection, in: Mater. Today Proc. - Recent Adv. Constr. Mater. Struct. ICCMS-2021, Elsevier, 2022, https://doi.org/10.1016/j.matpr.2022.04.140.
[14] T. Ribeiro, L. Bernardo, R. Carrazedo, D. De Domenico, Eurocode-compliant topology optimisation of steel moment splice connections, J. Build. Eng. 62 (2022), 105346, https://doi.org/10.1016/j.jobe.2022.105346.
[15] T. Ribeiro, L. Bernardo, R. Carrazedo, D. De Domenico, Ultimate capacity and stability of topologically optimised shear plates in compliance with structural Eurocodes, Structures 57 (2023), https://doi.org/10.1016/j.istruc.2023.105307.

[16] H.F. Isleem, N.D.K.R. Chukka, A. Bahrami, S. Oyebisi, R. Kumar, T. Qiong, Non-linear finite element and analytical modelling of reinforced concrete filled steel tube columns under axial compression loading, Results Eng (2023), https://doi.org/10.1016/j.rineng.2023.101341.
[17] S. Senapati, K.K. Sangle, Non-linear static analysis of cold-formed steel frame with rigid connections, Results Eng (2022), https://doi.org/10.1016/j.rineng.2022.100503.
[18] F. Sheikh-Ibrahim, Development of Design Procedures for Steel Girder Bolted Splices, The University of Texas at Austin, 1995.
[19] F.I. Sheikh-Ibrahim, K.H. Frank, The ultimate strength of symmetric beam bolted splices, Eng. J. 38 (2001) 100–117.
[20] C. Richter, Behavior of a Steel Girder Bolted Splice Connection, US Department of Transportation, Federal Highway Administration, McLean, 2017.
[21] ASTM, A36/A36M - 19, Standard Specification for Carbon Structural Steel, 2019.
[22] ASTM, A572/A572M − 15: High-Strength Low-Alloy Columbium-Vanadium Structural Steel, 2015.
[23] CEN, Eurocode 3, Design of Steel Structures - Part 1-1, General rules and rules for buildings, 2005.
[24] CEN, Eurocode 3, Design of Steel Structures - Part 1-8: Design of Joints, 2005.
[25] CEN, EN 1993-1-5, Eurocode 3 - Design of Steel Structures - Part 1-5, Plated structural elements, 2006.
[26] V.S. Barbosa, C. Ruggieri, Effects of increased span on fracture toughness using non-standard PCVN specimens and implications for the reference temperature, T 0, Procedia Struct. Integr. 13 (2018) 367–372, https://doi.org/10.1016/j.prostr.2018.12.061.
[27] C. Rex, W. Samuel Easterling, Behavior and Modeling of Mild and Reinforcing Steel, 1996.
[28] K. Jiang, O. Zhao, K.H. Tan, Experimental and numerical study of S700 high strength steel double shear bolted connections in tension, Eng. Struct. 225 (2020), 111175, https://doi.org/10.1016/j.engstruct.2020.111175.
[29] K. Jiang, K.H. Tan, O. Zhao, L. Gardner, Block tearing of S700 high strength steel bolted connections: testing, numerical modelling and design, Eng. Struct. 246 (2021), 112979, https://doi.org/10.1016/j.engstruct.2021.112979.
[30] H. Cheng, C.M. Paz, B.C. Pinheiro, S.F. Estefen, Experimentally based parameters applied to concrete damage plasticity model for strain hardening cementitious composite in sandwich pipes, Mater. Struct. Constr. (2020), https://doi.org/10.1617/s11527-020-01513-9.
[31] A.M. Sousa, H.A. Matos, M.J. Pereira, Properties of crude oil-in-water and water-in-crude oil emulsions: a critical review, Ind. Eng. Chem. Res. (2022), https://doi.org/10.1021/acs.iecr.1c02744.
[32] M. Kořínek, R. Halama, F. Fojtík, M. Pagáč, J. Krček, D. Krzikalla, R. Kocich, L. Kunčická, Monotonic tension-torsion experiments and fe modeling on notched specimens produced by slm technology from ss316l, Materials (2021), https://doi.org/10.3390/ma14010033.